



RESEARCH ARTICLE

Lactate Production Precedes Inflammatory Cell Recruitment in Arthritic Ankles: an Imaging Study

Marie-Aline Neveu,¹ Nicolas Beziere,¹ Rolf Daniels,² Caroline Bouzin,³
Arnaud Comment,⁴ Johannes Schwenck,^{1,5,6} Kerstin Fuchs,¹ Manfred Kneilling,^{1,6,7}
Bernd J. Pichler,^{1,6} Andreas M. Schmid ¹

¹Werner Siemens Imaging Center, Department of Preclinical Imaging and Radiopharmacy, Eberhard Karls University Tuebingen, Roentgenweg 13, 72076, Tuebingen, Germany

²Department of Pharmaceutical Technology, Eberhard Karls University Tuebingen, Tuebingen, Germany

³IREC Imaging Platform, Institute of Experimental and Clinical Research, Université catholique de Louvain, Brussels, Belgium

⁴General Electric Healthcare, Pollards Wood, Nightingales Lane, Chalfont St Giles, UK

⁵Department of Nuclear Medicine and Clinical Molecular Imaging, Eberhard Karls University Tuebingen, Tuebingen, Germany

⁶Cluster of Excellence iFIT (EXC 2180) “Image-Guided and Functionally Instructed Tumor Therapies”, University of Tuebingen, Tuebingen, Germany

⁷Department of Dermatology, Eberhard Karls University Tuebingen, Tuebingen, Germany

Abstract

Purpose: Inflammation is involved in many disease processes. However, accurate imaging tools permitting diagnosis and characterization of inflammation are still missing. As inflamed tissues exhibit a high rate of glycolysis, pyruvate metabolism may offer a unique approach to follow the inflammatory response and disease progression. Therefore, the aim of the study was to follow metabolic changes and recruitment of inflammatory cells after onset of inflammation in arthritic ankles using hyperpolarized 1-¹³C-pyruvate magnetic resonance spectroscopy (MRS) and ¹⁹F magnetic resonance imaging (MRI), respectively.

Procedure: Experimental rheumatoid arthritis (RA) was induced by intraperitoneal injection of glucose-6-phosphate-isomerase-specific antibodies (GPI) containing serum. To monitor pyruvate metabolism, the transformation of hyperpolarized 1-¹³C-pyruvate into hyperpolarized 1-¹³C-lactate was followed using MRS. To track phagocytic immune cell homing, we intravenously injected a perfluorocarbon emulsion 48 h before imaging. The animals were scanned at days 1, 3, or 6 after GPI-serum injection to examine the different stages of arthritic inflammation. Finally, to confirm the pyruvate metabolic activity and the link to inflammatory cell recruitment, we conducted hematoxylin-eosin histopathology and monocarboxylase transporter (MCT-1) immune histochemistry (IHC) of inflamed ankles.

Manuscript submitted as an original article to *Molecular Imaging and Biology*

Electronic supplementary material The online version of this article (<https://doi.org/10.1007/s11307-020-01510-y>) contains supplementary material, which is available to authorized users.

Correspondence to: Andreas Schmid; e-mail: a.schmid@med.uni-tuebingen.de

Results: Hyperpolarized 1-¹³C-pyruvate MRS revealed a high rate of lactate production immediately at day 1 after GPI-serum transfer, which remained elevated during the progression of the disease, while ¹⁹F-MRI exhibited a gradual recruitment of phagocytic immune cells in arthritic ankles, which correlated well with the course of ankle swelling. Histopathology and IHC revealed that MCT-1 was expressed in regions with inflammatory cell recruitment, confirming the metabolic shift identified in arthritic ankles.

Conclusions: Our study demonstrated the presence of a very early metabolic shift in arthritic joints independent of phagocytic immune cell recruitment. Thus, hyperpolarized 1-¹³C-pyruvate represents a promising tracer to monitor acute arthritic joint inflammation, even with minor ankle swelling. Furthermore, translated to the clinics, these methods add a detailed characterization of disease status and could substantially support patient stratification and therapy monitoring.

Key Words: Rheumatoid arthritis, Lactate, Hyperpolarized ¹³C-MRS, ¹⁹F-MRI, Immune imaging

Introduction

Rheumatoid arthritis (RA) is an autoimmune disease affecting 1–2 % of the worldwide population and causes severe disabilities. The disease is characterized by a dense inflammatory cell infiltrate in the joints, proliferation of synovial cells, angiogenesis, and pannus formation. This chronic inflammation of the synovial tissues leads to cartilage and bone destruction, and ultimately to joint deformity and infirmity [1]. Thus, early diagnosis is essential to rapidly initiate anti-inflammatory treatment approaches with steroids, nonsteroidal anti-inflammatory drugs, or biologicals (anti-TNF mAbs, anti IL-17 mAbs) in order to limit tissue damage, especially in juvenile RA. The current diagnostic tools in patients rely on clinical examination, blood tests, radiography, power Doppler ultrasonography, computed tomography, or magnetic resonance imaging (MRI), but unfortunately lack specificity and are only capable of identifying rather advanced stages of arthritic joint diseases [2]. Consequently, there is a critical need for robust diagnostic methods that are able to identify early inflammatory processes within the inflamed joints, even before severe joint and cartilage destruction.

Metabolic reprogramming is a key feature of inflamed tissues, typically associated with reduced oxidation while favoring glycolysis and glutaminolysis [3], leading to high glucose demand, high lactate levels, and acidosis, directly contributing to cellular injury *via* proinflammatory signals [4, 5]. While early metabolic changes in RA and the effects of anti-inflammatory treatment approaches can be monitored by molecular imaging using the gold standard 2-deoxy-2-[¹⁸F]fluoro-D-glucose (¹⁸F-FDG) positron emission tomography (PET) [6–9], only two studies investigated lactate production in preclinical models of RA but exclusively examined the advanced severe stage using hyperpolarized 1-¹³C-pyruvate magnetic resonance spectroscopic imaging (MRSI) [10, 11]. In our studies, we examined the glucose-6-phosphate-isomerase (GPI)-serum-induced experimental RA to monitor the temporal dynamics of the effector phase of arthritic joint disease [12]. GPI-serum-induced experimental RA is independent of T and B cells, and is characterized by polymorphonuclear cell and macrophage recruitment specific to the sites of arthritic joints [13–15] and is best qualified to study

the effector phase of acute arthritic joint disease, as it shares multiple similarities with the effector phase of RA in patients.

The aim of our study was to noninvasively monitor the transformation of hyperpolarized 1-¹³C-pyruvate into hyperpolarized 1-¹³C-lactate *in vivo* over time [16] and to determine its interplay with the temporal dynamics of phagocytic immune cell recruitment (phagocytes, such as macrophages) during the development of experimental RA with a perfluorocarbon (PFC) emulsion using ¹⁹F magnetic resonance imaging (¹⁹F-MRI) [17].

Materials and Methods

Animal Model of Arthritis

Acute GPI-serum-induced arthritis was induced as described previously [12, 18, 19]. Briefly, GPI-serum was obtained from generation 1 (K/BxN mice 1–3 months old) and diluted 1:1 (v/v) with saline before injection. Two hundred microliters of either diluted GPI-serum ($n=26$) or saline ($n=11$) was injected intraperitoneally into randomized groups of 8- to 12-week-old female BALB/c mice (Charles River GmbH, Erkrath, Germany). Control-serum was collected from healthy C57BL/6 mice. Caliper measurements of the ankle diameter (hind legs) were performed before serum transfer and at the indicated time points after serum transfer to follow ankle swelling.

Different cohorts of mice were examined with hyperpolarized ¹³C-MRS, ¹⁹F-MRI, or histology at days 1, 3, or 6 after GPI-serum injection to follow the early, moderate, and severe stages of inflammation in this model [18, 19]. Control animals were imaged on day 9 after saline injection.

MRS and MRI measurements were performed on a dedicated 7 T small animal MRI (BioSpec, Bruker BioSpin GmbH, Ettlingen, Germany) controlled by Paravision 6.0.1 (BrukerBioSpin GmbH). During experiments, the animals were anesthetized by the inhalation of isoflurane (Forene, Abbot, England) evaporated in 100 % O₂ and warmed using a circulating water system. All applicable institutional and/or national guidelines for the care and use of animals were followed.

Hyperpolarized ^{13}C -MRS

For hyperpolarized ^{13}C -MRS measurements, the animals were fasted overnight. $1\text{-}^{13}\text{C}$ -pyruvate solutions were hyperpolarized using a DNP polarizer (SpinLab, General Electric, Waukesha, USA). $\text{C}1$ -labeled pyruvic acid (Cortecnet, Voisins-le-Bretonneux, France) was polarized according to the manufacturer's instructions. After 60–90 min, the hyperpolarized sample was rapidly dissolved and neutralized in an aqueous solution containing 40 mM Tris, 60 mM NaOH, and 0.1 g/L Na_2EDTA . The hyperpolarized $1\text{-}^{13}\text{C}$ -pyruvate solution (80 mM) was intravenously injected through a catheter placed in the tail vein of the animal.

Both hind legs of the animal were positioned on a $^1\text{H}/^{13}\text{C}$ surface coil (2 cm in diameter, Bruker BioSpin GmbH). Started directly before the injection of the hyperpolarized $1\text{-}^{13}\text{C}$ -pyruvate solution, coil-localized ^{13}C spectra of the ankles were acquired every second for 240 s using a single pulse sequence (Bandwidth: 3019.32 Hz; α : 5° ; 1024 points).

Using jMRUI v5, a zero-order phase correction was manually applied, and a 50 Hz apodization filter was executed on the time series. The data were then analyzed based on a model free-approach using the lactate-to-pyruvate ratio (Lac/Pyr) [20] calculated from the total areas under the dynamic curves of the $1\text{-}^{13}\text{C}$ -lactate and $1\text{-}^{13}\text{C}$ -pyruvate phased signals.

Apparent decay constants were fit to the decreasing part of the normalized peak using a mono-exponential function (Prism 7, GraphPad Software, San Diego, CA, USA). Values where a 95 % confidence interval could not be provided were excluded from the analysis ($n = 3$).

^{19}F -MRI

For generation of the ^{19}F -PFC emulsion, 10 % wt/wt perfluoro-15-crown-5 ether (Fluorochem, Derbyshire, UK) and 4 % wt/wt purified egg lecithin E80S (Lipoid, Ludwigshafen, Germany) were mixed in isotonic buffer (10 mM HEPES, 2.5 % glycerol, pH 7.4) to yield a coarse raw emulsion [21]. This raw emulsion was homogenized with a high-pressure (75 MPa, 10 cycles) Emulsiflex C5 homogenizer (Avestin, Mannheim, Germany). A final particle size of 110 ± 5 nm was achieved, as determined by dynamic light scattering using a Zetasizer Nano-ZS (Malvern Instruments Ltd., Malvern, UK).

The ^{19}F -PFC emulsion was administered intravenously to the animals at 48 h before ^{19}F -MRI detection using an infusion pump (100 $\mu\text{l}/\text{min}$ for 5 min) to track the accumulation of phagocytic cells at the site of inflammation.

Animals were placed in a ^1H - ^{19}F transmit-receive volume coil (inner diameter of 40 mm, Bruker BioSpin GmbH). ^{19}F axial images of the hind legs were obtained using a rapid acquisition with relaxation enhancement (RARE) sequence

(repetition time (TR), 3000 ms; echo time (TE), 7.65 ms; RARE factor, 17; field of view (FOV), 40×40 mm²; slice thickness, 2 mm; number of averages (NA), 180; acquisition time, 9 min). ^1H reference images were obtained using a T2-weighted 3-dimensional RARE sequence (TE/TR, 30.82/800 ms; RARE factor, 16; FOV, $60 \times 32 \times 23$ mm³). The $^1\text{H}/^{19}\text{F}$ MRI images were fused and analyzed using PMOD 3.2 software (PMOD Technologies Ltd., Zurich, Switzerland). The ^{19}F signal was determined similarly to the method presented by Temme *et al* [21]. The 2D regions of interest (ROIs) were drawn on consecutive axial slices covering the legs from palms to knees. The integrated intensity within the ROIs was then calculated for each leg of the animals. Overlays of the $^1\text{H}/^{19}\text{F}$ images were generated using Inveon Research Workplace software (Siemens Healthineers, Erlangen, Germany).

Histology and Immunohistochemistry

After sacrifice, both hind limbs were dissected and fixed immediately for 24 h in 4 % paraformaldehyde. Tissue samples were then decalcified in 10 % EDTA for 10 days, followed by 3 days in a decalcifying solution (OsteoRAL R fast decalcifier, VWR International Ltd., Leicestershire, UK) at room temperature with continuous agitation before paraffin embedding. The tissues were cut into 5 μm sections before staining. Hematoxylin and eosin (H&E) staining was performed following standard procedures. Tissue sections were also stained for monocarboxylate transporter 1 (MCT-1) (rabbit anti-MCT1, Sigma-Aldrich, St. Louis, USA). The DakoEnVision+ anti-rabbit kit (Agilent Technologies, Santa Clara, USA) was used to detect primary antibodies. Stained slides were digitalized using a SCN400 slide scanner (Leica Biosystems, Wetzlar, Germany).

Statistical Analysis

Analysis was performed using GraphPad Prism 7 software. The results are expressed as the mean value \pm SEM. One-way ANOVA with Dunnett's test *post hoc* was performed to investigate any mean difference over time of thickness in arthritic or control ankles. An unpaired t-test was used to compare the mean signal changes in the arthritic and control ankles. All statistical tests were two-sided, with $p < 0.05$ (*), $p < 0.01$ (**), or $p < 0.001$ (***) considered significant.

Results

Lactate Production Peaks before Maximal Joint Swelling

Hyperpolarized ^{13}C -MRS was performed on different cohorts of animals on days 1, 3, or 6 after GPI-serum injection to examine lactate production during the early and severe stages of inflammation in this acute model of arthritis (Fig. 1). A

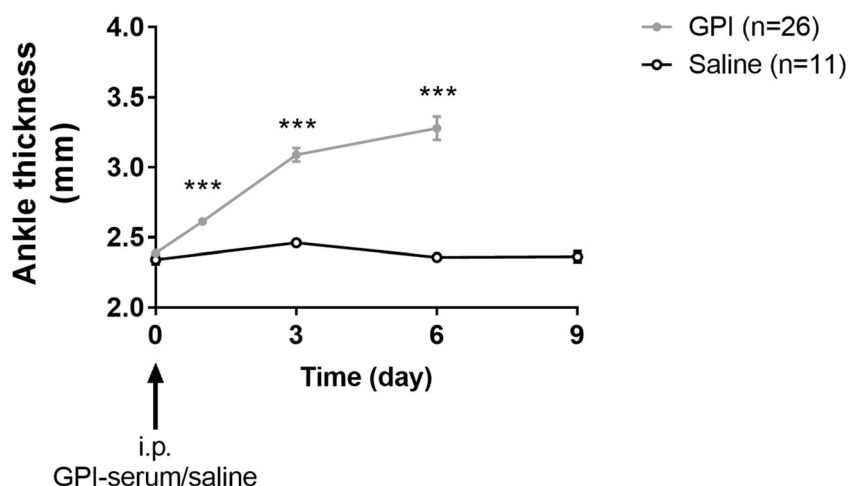


Fig. 1 Course of ankle swelling. A significant increase in ankle thickness was observed in GPI-serum injected mice ($n = 26$), while ankles of saline injected animals ($n = 11$) remained unaffected ($p < 0.001$). Hyperpolarized ^{13}C -MRS and ^{19}F -MRI were performed on different cohorts of animals at day 1, day 3, or day 6 after GPI-serum injection (indicated by gray arrows) to follow the early and severe stages of inflammation in this model. Control animals were scanned at day 9 after saline injection (indicated by a black arrow). Data are expressed as the mean \pm SEM. One-way ANOVA was used to follow the course ankle swelling in each group (each time point compared with day 0).

significant increase in ankle thickness was already observed after day 1 in GPI-serum-injected mice compared with baseline. This effect was followed by the expansion of the swelling until day 6 ($n = 26$; $p < 0.0001$). The ankles of saline-injected animals remained unaffected ($n = 11$; $p = 0.1378$). All animal cohorts used for this study demonstrated similar ankle swellings as previously reported [18, 19].

Evolution of lactate signal in the ankles typically differentiates arthritic (Fig. 2a–c) and control (Fig. 2d, Supplemental Fig. S1) mice during hyperpolarized $1\text{-}^{13}\text{C}$ -pyruvate MRS experiments. In GPI-serum-injected animals, the lactate signal was visibly increased at all time points and correlated with a higher pyruvate signal, while both signals remained at baseline in saline-injected animals. After GPI-serum transfer, an elevated Lac/Pyr ratio, reflecting lactate production, was immediately identified at day 1 (Fig. 3). The mean Lac/Pyr ratio shifted from 0.57 ± 0.11 at day 1 ($n = 3$; $p = 0.0407$) to 0.55 ± 0.10 at day 3 ($n = 4$; $p = 0.0429$) and to 0.45 ± 0.06 at day 6 ($n = 5$; $p = 0.0743$) when compared with control ankles, exhibiting a ratio of 0.23 ± 0.04 ($n = 4$). Interestingly, lactate production peaked as early as 1 day after the GPI-serum transfer when hardly any ankle swelling was detectable. Notably, the time-to-peak for lactate production was fastest at day 1 and increased with disease progression (Fig. 2, Supplemental Fig. S2); however, this effect was not significant compared with the control group. The apparent decays from the average of all RA (control) spectra were 24.0 ± 1.9 s (18.5 ± 1.2 s) and 46.6 ± 2.1 s (26.4 ± 6.6 s) for hyperpolarized $1\text{-}^{13}\text{C}$ -Pyruvate and hyperpolarized $1\text{-}^{13}\text{C}$ -Lactate, respectively.

Immune Cell Recruitment Follows the Course of Ankle Swelling

To identify a link between the dynamics of lactate production and immune cell recruitment in our model, ^{19}F -MRI measurements were performed after the injection of a PFC emulsion on a different cohort of animals. Subsequently, ^{19}F images were fused with corresponding ^1H anatomical images of arthritic (Fig. 4a–c) and unaffected naïve (Fig. 4d) ankles of GPI-serum-injected or healthy experimental mice. Merged images revealed a clear PFC accumulation in both paws of arthritic animals at day 3 (Fig. 4b) and day 6 (Fig. 4c). Twenty-four hours after the onset of GPI-serum-induced arthritis, we observed no enhancement of the ^{19}F signal (56.7 ± 5.3 ; $n = 4$; $p = 0.1254$), whereas on day 3, a significant increase was observed in the arthritic ankles (118.6 ± 10.8 ; $n = 2$; $p = 0.0056$) compared with the healthy control ankles (71.3 ± 7.4 ; $n = 3$) (Fig. 5). On day 6, a 7.1-fold enhancement of the ^{19}F signal was observed in the arthritic ankles (506.3 ± 40.3 ; $n = 4$; $p < 0.0001$) when compared with the ankles of healthy mice. In arthritic ankles, a gradual increase of the ^{19}F signal was observed between day 1, day 3 (2.1-fold increase between day 1 and day 3; $p = 0.0002$), and day 6 (8.9-fold increase between day 1 and day 6; 4.3-fold increase between day 3 and day 6; $p < 0.0001$ both). The quantification of the ^{19}F signal in the ankles reveals a progressive immune cell recruitment in arthritic animals that correlates with the course of ankle swelling.

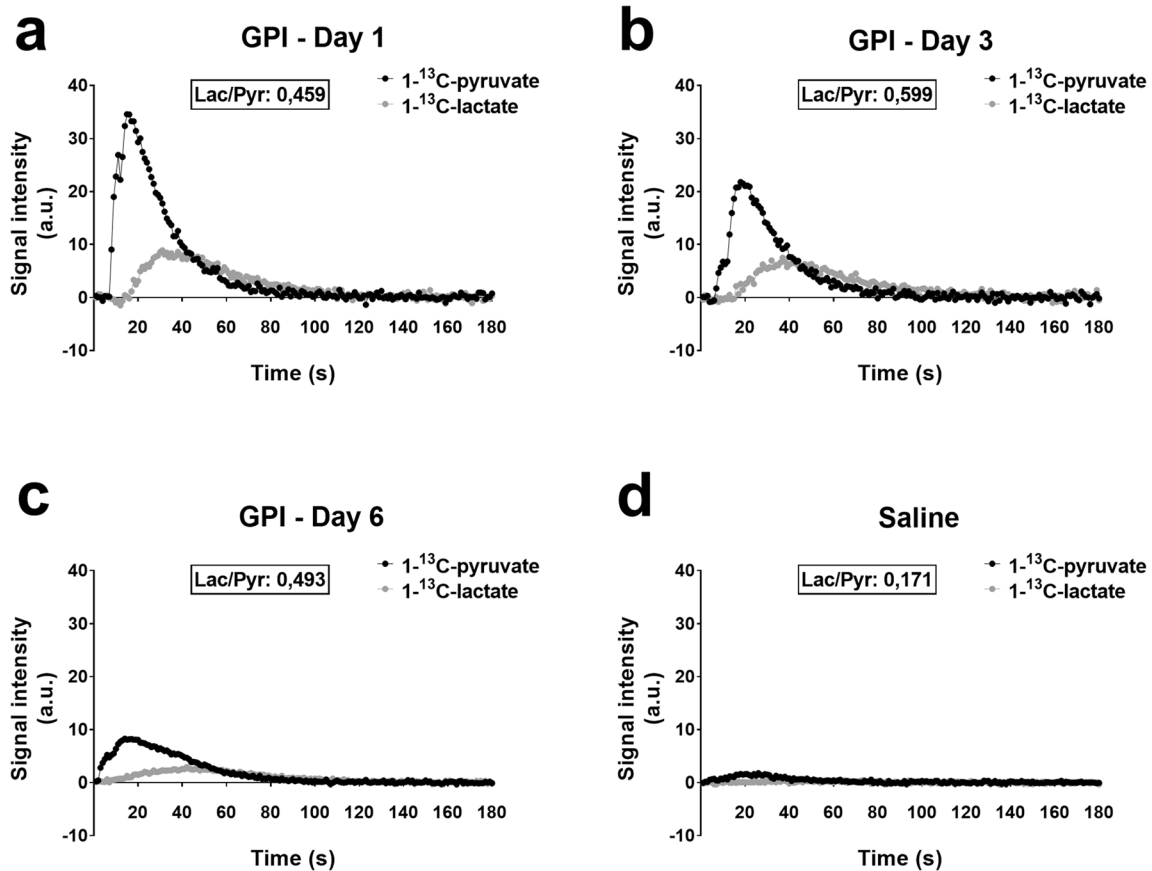


Fig. 2 Hyperpolarized $1\text{-}^{13}\text{C}$ -pyruvate-MRS reveals lactate formation in arthritic ankles. Representative pyruvate and lactate time intensity curves after i.v. injection of hyperpolarized $1\text{-}^{13}\text{C}$ pyruvate from representative arthritic (a–c) and control (d) ankles. The lactate-to-pyruvate (lac/Pyr) ratio, representing lactate production, was quantified based on the areas under the curves of the $1\text{-}^{13}\text{C}$ -lactate and $1\text{-}^{13}\text{C}$ -pyruvate signal intensities. A.u., Arbitrary units.

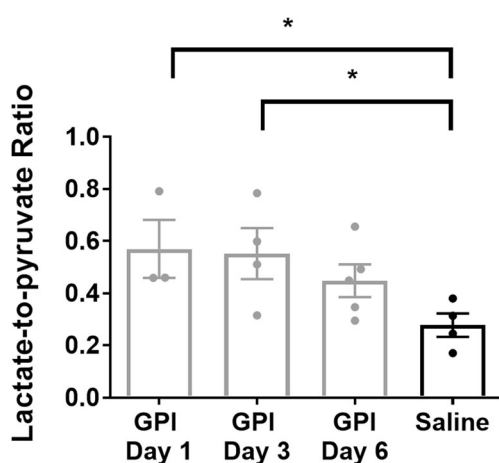


Fig. 3 Quantification of $1\text{-}^{13}\text{C}$ -pyruvate transformation into $1\text{-}^{13}\text{C}$ -lactate reveals an early metabolic shift occurring in arthritic ankles. Lactate production, measured by the lactate-to-pyruvate ratio, is at the highest level early in the disease (GPI day 1) and decreases with later stages. Individual values per animal are displayed as dots. Data are expressed as the mean \pm SEM. Unpaired t-tests were two-sided. $n = 3\text{--}5$ mice/group. A.u., Arbitrary units.

MCT-1 Staining Supports an Early Metabolic Shift Identified in Arthritic Ankles

To confirm the inflammatory response and the link with pyruvate metabolic activity in synovial membrane tissues of arthritic ankles, the expression of the MCTs was evaluated in parallel with H&E staining (Fig. 6). The initiation of histological changes, including immune cell infiltration and hyperplasia of the synovial membrane, was identified at day 1 after GPI-serum administration (Fig. 6a, left-hand side and center), with a progression of pannus formation until day 6. At this stage of the disease, a dense immune infiltration was observed in the synovium and the subsynovial pericapsular tissue (synovitis) (Fig. 6c, left-hand side and center). Strong peri-arthritis was also observed in the subcutaneous tissue adjacent to the joint. These observations were consistent with our previous studies on this model [18] and correlated with the *in vivo* ^{19}F -MRI results. Immunohistochemical staining showed limited MCT-1 expression in the control ankles with staining patterns in the skin and the subcutaneous tissue adjacent to the joint (Fig. 6d, right-hand side). In the arthritic ankles (Fig. 6a–c, right-hand side), the regions with inflammatory cell recruitment, such as the synovitis and

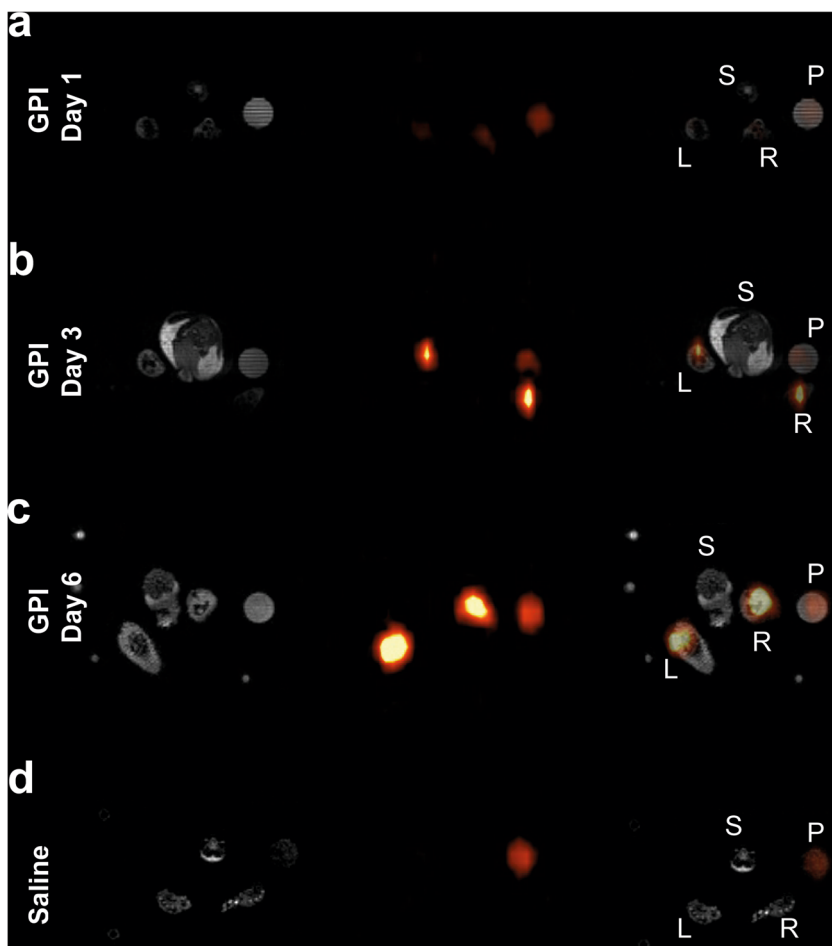


Fig. 4 ^{19}F -MRI exhibits PFC accumulation in arthritic ankles of GPI-serum injected mice. Representative anatomical ^1H images (grayscale), ^{19}F images (pseudocolor) and merged $^1\text{H}/^{19}\text{F}$ images for visualization PFC accumulation into arthritic (a–c) and control (d) ankles. The PFC emulsion was injected 2 days prior to imaging. ^{19}F axial slices are identically scaled. Labels are S = spine, P = reference phantom, L = left leg, R = right leg.

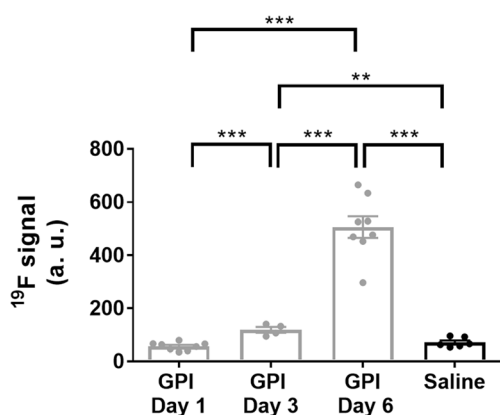


Fig. 5 Quantification of the ^{19}F signal highlights progressive immune cell recruitment in arthritic ankles. Measurements of individual legs are presented. While at day 1 macrophage levels in arthritic ankles are comparable to the control ankles, a continuous increase in ^{19}F -PFC signal is evident following ankle swelling. Data are expressed as the mean \pm SEM. Unpaired t-tests were two-sided. $n = 2\text{--}4$ mice/group. A.u., Arbitrary units.

the periarticular regions, expressed MCT-1 and correlated with the severity of the disease supporting the presence of a high metabolic activity in the inflamed regions. As MCT-1 is responsible for the transport of hyperpolarized $1\text{-}^{13}\text{C}$ -pyruvate and has been characterized as one of the limiting factors for its kinetic conversion into lactate [22, 23], the limited expression of MCT-1 in control ankles reflects the restricted pyruvate signal and lactate conversion observed by ^{13}C -MRS (Fig. 2d, Fig. 3) and confirms the metabolic shift identified in arthritic ankles (Fig. 2a–c, Fig. 3).

Discussion

By following the course of lactate production during the progression of arthritis, we identified an early peak of lactate that was associated with limited immune cell infiltration in arthritic ankles. Our previous imaging studies on GPI-serum-induced arthritis revealed that the course of ankle swelling was associated with increased cellular proliferation, followed by $3'\text{-deoxy-3'-}[^{18}\text{F}]\text{-fluorothymidine}$ (^{18}F -FLT) PET [18].

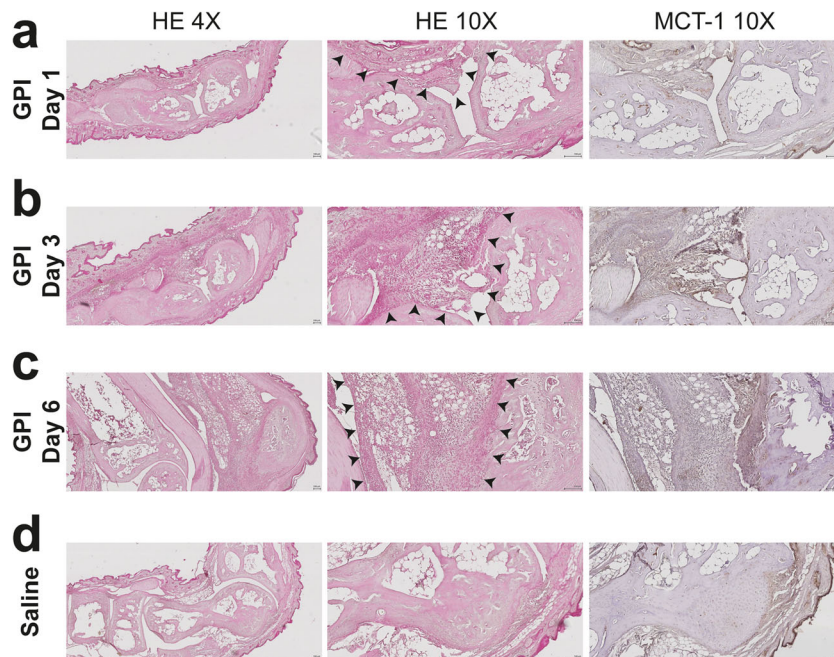


Fig. 6 Histological analysis confirms leucocyte accumulation and enhanced metabolic activity in arthritic ankles. Representative H&E and MCT-1 stained slices of arthritic (a-c) and control (d) ankles. While no signs of inflammation were identified in control ankles, arthritic ankles revealed increasing inflamed regions (indicated by arrowheads) on H&E stained slices (left and center panels). MCT-1 staining (right panels) demonstrated increased enzyme expression in the inflamed regions of arthritic ankles.

Additionally, [^{18}F]-fluoromisonidazole (^{18}F -FMISO) and [^{18}F]-fluoroazomycinaraboside (^{18}F -FAZA) PET probes revealed an early onset of hypoxia at day 3 post-GPI-serum transfer [19] that was associated with enhanced $\alpha_v\beta_3$ integrin activity, as determined by [^{18}F]-galacto-RGD PET [12], revealing angiogenesis in the diseased ankles. Finally, reactive oxygen species (ROS) stress was identified as maximal during the severe phase of the disease at day 6 [19] by using a ROS-sensitive chemiluminescence optical imaging probe L-012. As ROS are mainly generated by neutrophils and macrophages during inflammation, both cell types are critically involved in experimental GPI-serum-induced arthritis [14, 15, 24], we hypothesized that the progression of the disease could be driven by the progressive recruitment of active inflammatory cells into the joints, leading first to hypoxia and finally to ROS production. We wanted to correlate immune cell recruitment with the presence of a glycolytic phenotype in the joints of this experimental RA model. Interestingly, our studies revealed that an early metabolic shift uncovered by the determination of increased lactate production in inflamed ankles precedes pronounced phagocytic immune cell recruitment.

The metabolic shift occurring during joint inflammation has been previously revealed using molecular imaging such as ^{18}F -FDG PET and hyperpolarized $1\text{-}^{13}\text{C}$ -pyruvate MRSI [10, 11]. In a nonsystemic antigen-independent model of local severe experimental RA induced by a single

subcutaneous injection of complete Freund's adjuvant (CFA) into the hind paws, MacKenzie and colleagues assessed alterations in the conversion of hyperpolarized $1\text{-}^{13}\text{C}$ -pyruvate into $1\text{-}^{13}\text{C}$ -lactate, suggesting that this new tool may be used to indicate the presence of inflammatory arthritis [10]. Inflamed rat paws exhibited a Lac/Pyr ratio of 0.52 ± 0.16 (mean \pm SD) compared with control paws presenting a Lac/Pyr ratio of 0.32 ± 0.11 . More recently, Wright and coworkers confirmed these results in CFA-induced joint inflammation in mice [11]. A higher Lac/Pyr ratio of 0.74 ± 0.32 (mean \pm SD) was found in inflamed joints when measuring the entire signal coming from the inflamed feet of a small cohort of animals. While the results of both studies correlated with previous reports of increased lactate levels in the synovial fluid of RA patients [25, 26], only the severe phase of the arthritic joint disease was investigated when the joint swelling was maximal. Our hyperpolarized ^{13}C MRS data were consistent with the values reported by MacKenzie *et al* and Wright *et al* [10, 11]. We identified a Lac/Pyr ratio of 0.45 ± 0.06 (mean \pm SEM) in arthritic ankles during the severe phase at day 6 (Fig. 3). This effect was associated with a high ^{19}F -signal in the ankles (Fig. 5), showing a massive immune cell infiltrate that correlates with the swelling and the severity of the inflammation. However, when focusing on other time points, such as the early and moderate phase of the disease, we identified that lactate production in inflamed joints was higher than that during the

severe phase, with an increased Lac/Pyr ratio at day 1 (0.57 ± 0.11) (Fig. 3). Surprisingly, the enhanced lactate production in inflamed ankles did not correlate with a pronounced phagocytic immune cell infiltrate, as the ^{19}F -signal increased delayed at day 3 after the onset of experimental RA (Fig. 5).

While the ^{19}F -signal followed the course of ankle swelling and reflected our previous data where we identified a gradual increase of proliferation in the arthritic ankles using ^{18}F -FLT [18], highlighting the progressive immune cell infiltration during the progression of inflammation, lactate production was highest during the early stage of the disease, which was associated with limited immune cell recruitment. While synovial lactate levels are increased in patients with established RA [25, 26], our study noninvasively identified that lactate production is already increased during the onset of the disease. Thus, noninvasive determination of lactate production might represent a novel diagnostic tool opening a window of opportunity for immediate anti-inflammatory treatment at very early stages of RA, which is of utmost importance for long-term remission of RA [27]. Furthermore, our results showed that the glycolytic phenotype observed in the joints does not originate only from macrophages and neutrophils only and therefore also other cell types may undergo metabolic reprogramming during the disease. Among these, fibroblast-like synoviocytes (FLSs), normally resident into the joints, have recently been demonstrated to play a key role in both the initiation and perpetuation of the disease after activation [28]. Activated FLSs acquire a tumor-like and aggressive phenotype associated with metabolic reprogramming, as well as new functions, such as chemokine and cytokine production [28, 29], thus playing an active role in immune cell recruitment and bone distortion [30]. While further investigations of the role and behavior of FLSs during the early phase of the disease are necessary, our results strongly indicate the activity of resident cells such as FLS. Recently, SPECT and PET probes were described to study the impact of fibroblasts in RA by targeting the fibroblast activation protein (FAP) and displayed uptake into slightly inflamed joints, while ^{18}F -FDG uptake was only able to reveal severely inflamed joints in mice. Used in combination with technologies targeting immune cell dynamics, the role of all cell actors involved in the pathogenesis of RA could be revealed and linked to variations of metabolic activities occurring during disease evolution.

Given the growing use of hyperpolarized $1\text{-}^{13}\text{C}$ -pyruvate MRSI in patients [31], this technology could represent a valuable tool to noninvasively identify and monitor joint inflammation compared with invasive synovial fluid samplings or nonspecific blood tests, especially for juvenile patients or patients only partially fulfilling the classification criteria of RA.

Conclusion

By combining for the first time hyperpolarized $1\text{-}^{13}\text{C}$ -pyruvate MRS for metabolic profiling and ^{19}F -MRI for phagocytic immune cell tracking, we were able to noninvasively demonstrate the presence of an early metabolic shift

in arthritic ankles independently of phagocytic immune cell recruitment. In addition to the early diagnosis of RA, the combination of these novel technologies, potentially including [^{18}F]FLT-PET [19], could represent a unique platform to characterize disease stages by revealing metabolic perturbations before joint damage. Furthermore, this improves the monitoring of anti-inflammatory treatment approaches and could thereby limit the number of patients disabled by joint destruction.

Acknowledgments. Open Access funding provided by Projekt DEAL. The authors would like to thank Michele De Beukelaer for excellent technical support performing the histology and the immunostainings. Further, the authors thank Dr. Ulrich Flögel for helpful discussion on ^{19}F -MRI.

Funding Information. This work was supported by the Werner Siemens-Foundation and funded by the Deutsche Forschungsgemeinschaft (DFG, German Research Foundation) under Germany's Excellence Strategy – EXC 2180–390900677.

Compliance with Ethical Standards

Conflict of Interest

A.C. is employed by General Electric Medical Systems Inc. The other authors declare that they have no conflict of interest.

Open Access This article is licensed under a Creative Commons Attribution 4.0 International License, which permits use, sharing, adaptation, distribution and reproduction in any medium or format, as long as you give appropriate credit to the original author(s) and the source, provide a link to the Creative Commons licence, and indicate if changes were made. The images or other third party material in this article are included in the article's Creative Commons licence, unless indicated otherwise in a credit line to the material. If material is not included in the article's Creative Commons licence and your intended use is not permitted by statutory regulation or exceeds the permitted use, you will need to obtain permission directly from the copyright holder. To view a copy of this licence, visit <http://creativecommons.org/licenses/by/4.0/>.

Publisher's Note. Springer Nature remains neutral with regard to jurisdictional claims in published maps and institutional affiliations.

References

1. Smolen JS, Aletaha D, Barton A, Burmester GR, Emery P, Firestein GS, Kavanaugh A, McInnes IB, Solomon DH, Strand V, Yamamoto K (2018) Rheumatoid arthritis. *Nat Rev Dis Primers* 4:18001
2. Suresh E (2004) Diagnosis of early rheumatoid arthritis: what the non-specialist needs to know. *J R Soc Med* 97:421–424
3. Geeraerts X, Bolli E, Fendt S-M, Van Ginderachter JA (2017) Macrophage metabolism as therapeutic target for Cancer, atherosclerosis, and obesity. *Front Immunol* 8 <https://doi.org/10.3389/fimmu.2017.00289>
4. Weyand CM, Goronzy JJ (2017) Immunometabolism in early and late stages of rheumatoid arthritis. *Nat Rev Rheumatol* 13:291–301
5. Rhoads JP, Major AS, Rathmell JC (2017) Fine tuning of immunometabolism for the treatment of rheumatic diseases. *Nat Rev Rheumatol* 13:313–320
6. Irmeler IM, Opfermann T, Gebhardt P, Gajda M, Bräuer R, Saluz HP, Kamradt T (2010) In vivo molecular imaging of experimental joint inflammation by combined ^{18}F -FDG positron emission tomography and computed tomography. *Arthritis Res Ther* 12:R203
7. Brenner W (2004) ^{18}F -FDG PET in rheumatoid arthritis: there still is a long way to go. *J Nucl Med* 45:927–929

8. Matsui T, Nakata N, Nagai S, Nakatani A, Takahashi M, Momose T, Ohtomo K, Koyasu S (2009) Inflammatory cytokines and hypoxia contribute to 18F-FDG uptake by cells involved in pannus formation in rheumatoid arthritis. *J Nucl Med* 50:920–926
9. Okamura K, Yonemoto Y, Arisaka Y, Takeuchi K, Kobayashi T, Oriuchi N, Tsushima Y, Takagishi K (2012) The assessment of biologic treatment in patients with rheumatoid arthritis using FDG-PET/CT. *Rheumatology* 51:1484–1491
10. MacKenzie JD, Yen Y-F, Mayer D, Tropp JS, Hurd RE, Spielman DM (2011) Detection of inflammatory arthritis by using hyperpolarized ¹³C-pyruvate with MR imaging and spectroscopy. *Radiology* 259:414–420
11. Wright AJ, Husson ZMA, Hu DE, Callejo G, Brindle KM, Smith ESJ (2018) Increased hyperpolarized [¹⁻¹³C] lactate production in a model of joint inflammation is not accompanied by tissue acidosis as assessed using hyperpolarized ¹³C-labelled bicarbonate. *NMR Biomed* 31:e3892
12. Kneilling M, Hültner L, Pichler BJ, Mailhammer R, Morawietz L, Solomon S, Eichner M, Sabatino J, Biedermann T, Krenn V, Weber WA, Illges H, Haubner R, Röcken M (2007) Targeted mast cell silencing protects against joint destruction and angiogenesis in experimental arthritis in mice. *Arthritis Rheum* 56:1806–1816
13. Asquith D, Miller A, McInnes I, Liew F (2009) Animal models of rheumatoid arthritis. *Eur J Immunol* 39:2040–2044
14. Wipke BT, Allen PM (2001) Essential role of neutrophils in the initiation and progression of a murine model of rheumatoid arthritis. *J Immunol* 167:1601–1608
15. Solomon S, Rajasekaran N, Jeisy-Walder E, Snapper SB, Illges H (2005) A crucial role for macrophages in the pathology of K/B_x N serum-induced arthritis. *Eur J Immunol* 35:3064–3073
16. Brindle KM (2015) Imaging metabolism with hyperpolarized (¹³C)-labeled cell substrates. *J Am Chem Soc* 137:6418–6427
17. Temme S, Bönner F, Schrader J, Flögel U (2012) 19F magnetic resonance imaging of endogenous macrophages in inflammation. *Wiley Interdiscip Rev Nanomed Nanobiotechnol* 4:329–343
18. Fuchs K, Kohlhofer U, Quintanilla-Martinez L, Lamparter D, Kotter I, Reischl G, Rocken M, Pichler BJ, Kneilling M (2013) In vivo imaging of cell proliferation enables the detection of the extent of experimental rheumatoid arthritis by 3'-deoxy-3'-18f-fluorothymidine and small-animal PET. *J Nucl Med* 54:151–158
19. Fuchs K, Kuehn A, Mahling M, Guenthoer P, Hector A, Schwenck J, Hartl D, Laufer S, Kohlhofer U, Quintanilla-Martinez L, Reischl G, Röcken M, Pichler BJ, Kneilling M (2017) In vivo hypoxia PET imaging quantifies the severity of arthritic joint inflammation in line with overexpression of hypoxia-inducible factor and enhanced reactive oxygen species generation. *J Nucl Med* 58:853–860
20. Hill DK, Orton MR, Mariotti E, Boulton JKR, Panek R, Jafar M, Parkes HG, Jamin Y, Miniotti MF, al-Saffar NMS, Belouche-Babari M, Robinson SP, Leach MO, Chung YL, Eykyn TR (2013) Model free approach to kinetic analysis of real-time hyperpolarized ¹³C magnetic resonance spectroscopy data. *PLoS One* 8:e71996
21. Temme S, Jacoby C, Ding Z, Bonner F, Borg N, Schrader J, Flögel U (2014) Technical advance: monitoring the trafficking of neutrophil granulocytes and monocytes during the course of tissue inflammation by noninvasive 19F MRI. *J Leukoc Biol* 95:689–697
22. Harris T, Eliyahu G, Frydman L, Degani H (2009) Kinetics of hyperpolarized ¹³C1-pyruvate transport and metabolism in living human breast cancer cells. *Proc Natl Acad Sci U S A* 106:18131–18136
23. Lodi A, Woods SM, Ronen SM (2013) Treatment with the MEK inhibitor U0126 induces decreased hyperpolarized pyruvate to lactate conversion in breast, but not prostate, cancer cells. *NMR Biomed* 26:299–306
24. Ji H, Ohmura K, Mahmood U, Lee DM, Hofhuis FMA, Boackle SA, Takahashi K, Holers VM, Walport M, Gerard C, Ezekowitz A, Carroll MC, Brenner M, Weissleder R, Verbeek JS, Duchatelle V, Degott C, Benoist C, Mathis D (2002) Arthritis critically dependent on innate immune system players. *Immunity* 16:157–168
25. Gobelet C, Gerster J (1984) Synovial fluid lactate levels in septic and non-septic arthritides. *Ann Rheum Dis* 43:742–745
26. Lenski M, Scherer MA (2014) The significance of interleukin-6 and lactate in the synovial fluid for diagnosing native septic arthritis. *Acta Orthop Belg* 80:18–25
27. Lard LR, Visser H, Speyer I, vander Horst-Bruinsma IE, Zwinderman AH, Breedveld FC, Hazes JMW (2001) Early versus delayed treatment in patients with recent-onset rheumatoid arthritis: comparison of two cohorts who received different treatment strategies. *Am J Med* 111:446–451
28. Korb-Pap A, Bertrand J, Sherwood J, Pap T (2016) Stable activation of fibroblasts in rheumatic arthritis—causes and consequences. *Rheumatology* 55:ii64–ii67
29. Müller-Ladner U, Ospelt C, Gay S, Distler O, Pap T (2007) Cells of the synovium in rheumatoid arthritis. *Synovial fibroblasts. Arthritis Res Ther* 9:223
30. Ospelt C, Gay S (2008) The role of resident synovial cells in destructive arthritis. *Best Pract Res Clin Rheumatol* 22:239–252
31. Kurhanewicz J, Vigneron DB, Ardenkjaer-Larsen JH, Bankson JA, Brindle K, Cunningham CH, Gallagher FA, Keshari KR, Kjaer A, Laustsen C, Mankoff DA, Merritt ME, Nelson SJ, Pauly JM, Lee P, Ronen S, Tyler DJ, Rajan SS, Spielman DM, Wald L, Zhang X, Malloy CR, Rizi R (2019) Hyperpolarized (¹³C) MRI: path to clinical translation in oncology. *Neoplasia* 21:1–16

Publisher's Note Springer Nature remains neutral with regard to jurisdictional claims in published maps and institutional affiliations.